Accepted Manuscript online: 2022-06-23 Article published online: 2022-07-14

Bifurcated Chalcogen Bonds Based on One σ-Hole

Saber Mehrparvar[a]
Christoph Wölper[a]
Rolf Gleiter*[b]
Gebhard Haberhauer*[a]

[a] Institut für Organische Chemie, Universität Duisburg-Essen, Universitätsstr. 7, 45117 Essen, Germany
[b] Organisch-Chemisches Institut, Universität Heidelberg, Im Neuenheimer Feld 270, 69120 Heidelberg, Germany
* rolf.gleiter@oci.uni-heidelberg.de; gebhard.haberhauer@uni-due.de

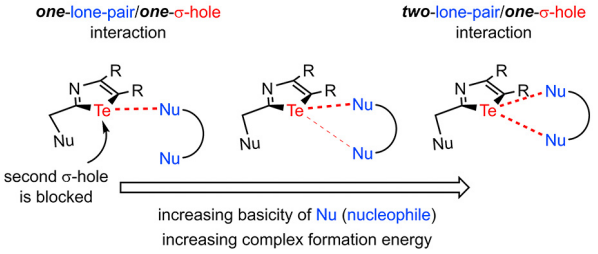

Received: 25.05.2022
Accepted after revision: 21.06.2022
DOI: 10.1055/a-1883-6076; Art ID: OM-2022-05-0005-OA

Abstract Chalcogen bonds are noncovalent interactions and are increasingly coming into focus for the design of complex structures in research areas such as crystal engineering, molecular recognition and catalysis. Conceptionally, chalcogen bonds can be considered as interaction between *one* σ-hole and *one* Lewis base center. Herein, we analyze the interaction between bidentate chelating ligands having *two* nucleophilic centers with *one* single σ-hole of a chalcogenazole (two-lone-pair/one-σ-hole interactions). Referring to this, we show by quantum chemical calculations and X-ray studies that three bond types are possible: in the first case, a chalcogen bond is formed between the σ-hole and only one of the Lewis base centers. In the second case, a strong bond is formed by one nucleophilic center; the second center provides only a small amount of additional stabilization. In the third case, two equivalent bonds to the σ-hole are formed by both Lewis base centers. According to the calculations, the bifurcated bonds are stronger than simple chalcogen bonds and lead to a more rigid molecular arrangement in the complex.

Key words: bifurcated bonds, chelate ligands, chalcogen bonding, DFT calculations, σ-hole

Introduction

In the last years, there has been an extremely rapid development in the field of chalcogen bonding.[1,2] Meanwhile, chalcogen bonds are employed in different research areas such as crystal engineering,[3–9] chalcogen-bonded organic frameworks,[10,11] molecular recognition in solution,[12–18] switches[19,20] and catalysis.[21–28] Chalcogen bonds, analogous to halogen bonds, are secondary bonds known as σ-hole interactions. These are noncovalent bonds between the σ-hole of one covalently bound atom of the IV–VII groups and one Lewis base lone pair.[29,30] The σ-hole is a region of positive electrostatic potential located on the extension of one of the covalent bonds to the atom.[29,30] Systematic investigations of chalcogen bonds revealed that the strength of the interaction strongly depends on the size of the chalcogen atom, the substituent at the chalcogen atom and the donor ability of the Lewis base.[31–33] Here, the following rule of thumb can be used: the larger the size of the chalcogen, the more electron-attracting the substituents at the chalcogen atoms, and the higher the donor ability of the Lewis base, the stronger is the corresponding chalcogen bond. Accordingly, particularly strong chalcogen bonds are found in electron-poor tellurium compounds such as isotellurazole oxides,[17,34] telluradiazoles[14,35,36] and tellurazoles.[37,38]

The most important components contributing to chalcogen bond strength are electrostatics, orbital mixing (induction interactions) and dispersion.[39] Which one of the three terms is contributing the most depends on the investigated systems. For example, the dispersion term is most important in $Me_2E\cdots EMe_2$ systems (E = chalcogen) and amounts to 70–90% of the sum of all attractive terms.[32,33] However, SAPT (symmetry-adapted intermolecular perturbation theory) calculations of chalcogen bonds in isotellurazole oxides, telluradiazoles and tellurazoles reveal that in general, the electrostatic term represents the main part of attractive interactions.[31] Especially in strong chalcogen bonds of tellurium-containing azoles, the dispersion energies only play a minor role.[31] However, experimental conformation studies of chalcogen-containing aromatics lead to the conclusion that the dominant interactions represent the $n \rightarrow \sigma^*$ orbital delocalization.[40] Two σ-hole effects are responsible for the orientation of the chalcogen bond, which is formed in extension of one of the covalent bonds to the chalcogen atom: the positive electrostatic potential and the low electron density. SAPT calculations show that the electrostatic interactions are crucial for the geometry of the chalcogen bond in sulfur- and selenium-containing aromatics, whereas in tellurium-containing aromatics bond geometries are affected by low steric interactions (Pauli repulsion) due to the low σ-hole electron density.[31]

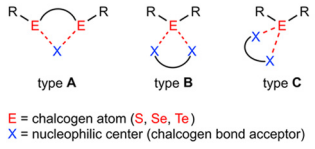

Figure 1 Possible bifurcated chalcogen bonds between divalent chalcogen atoms and nucleophilic centers (Lewis bases). In type B *two* nucleophilic centers interact with *two* σ-holes, whereas in type C *two* nucleophilic centers interact with *one* σ-hole.

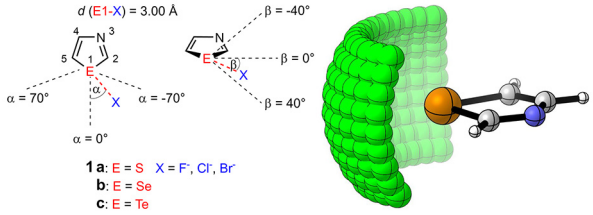

Figure 2 Definitions of the parameters *d*(E1-X), α and β in the model **1**•X to calculate interaction energy maps (left). Visualization of all possible orientations of chloride in the model **1c**•Cl^- (right).

The formation of complexes in which one of the two binding partners is bidental is highly interesting: due to the bidentate ligand bond rotation being restricted and the orientation of the two components in the complex is more fixed to each other. Divalent chalcogen centers exhibit two σ-holes and can therefore form different bifurcated bonds (Figure 1). In one case, two chalcogen atoms are connected to a nucleophilic center (type A); in the other case, two nucleophilic centers are bound to a chalcogen atom (type B).[41] Using the first strategy (type A), the anion transport with chalcogen bonds[18] and the anion recognition in water by charge-neutral chalcogen bonding foldamer receptors have been realized.[13] Using this second concept (type B), the synthesis of molecular capsules based on chalcogen bonds has been achieved.[14] Please note, in type B the two Lewis base centers interact with two σ-holes at one chalcogen atom.

In principle, there should be a third option for bifurcated chalcogen bonds, in which *two* nucleophilic centers interact with *one* σ-hole (type C in Figure 1). This bond type is a three-centered interaction and resembles that found in bifurcated hydrogen and halogen bonds.[42–44] Herein, we analyze by means of interaction energy maps of chalcogenazoles if one single σ-hole is theoretically able to form chalcogen bonds with more than one nucleophilic center and how these two centers have to be arranged to each other. Afterwards, we use quantum chemical calculations and X-ray studies to prove that tellurium-containing benzoazoles can form such two-lone-pair/one-σ-hole interactions.

Results and Discussion

a) Interaction Energy Maps of Chalcogen Bonds

In the first step, we wanted to generate interaction energy maps of model systems to analyze the angle dependency of the chalcogen bond and to check if the formation of two chalcogen bonds to one single σ-hole is generally possible. As reference systems for chalcogen bond donors we used chalcogenazoles due to their ability to form strong chalcogen bonds; furthermore, we already have experience regarding the synthesis and investigations of these systems.[10,31] As Lewis bases, the halides·F^-, Cl^- and Br^- were used. These anions have the advantage that they are spherical and monatomic. Therefore, calculations are simplified. If polyatomic Lewis bases were used, additional parameters such as the orientation of all atoms relative to the nucleophilic center must be considered.

Model **1**•X is defined by three parameters (Figure 2): the distance *d*(E1-X) between the halide X and the chalcogen center E1 and the angles α and β. Angle α is formed by the junction of two straight lines: one passes the centers E1 and X, and the other one passes E1 and the center between the atoms N3 and C4 (Figure 2). Angle β results from the junction of the straight line through the centers E1 and X and the straight line passing E1 and being parallel to the N3–C4 bond (Figure 2). The distance *d*(E1-X) was constantly fixed to the value obtained by optimizing the underlying system using the B2PLYP[45] approximation with additional dispersion correction.[46] The angles α and β were changed in 10° steps; α was variated from −70° to +70° and β from −40° to +40°. In Figure 2, all possible orientations of model **1c**•Cl^- are depicted. Each chloride corresponds to a conformation with specific α and β values.

For model calculations, the CCSD(T) approximation was applied. This method is renowned as the gold standard in the field of noncovalent bond determination.[47] The TZVP basis set was used for all atoms except tellurium. For the latter, the aug-cc-pVTZ-PP basis set was employed. To eliminate the basis set superposition error, the counterpoise method was applied.[48] The obtained energies are shown in Tables S1–S9. As expected, the energy values for the most favorable conformations increase with increasing chalcogen atom sizes and decreasing nucleophile sizes. Thus, the highest binding energies are found for **1c**•F^- (−37.2 kcal/mol) and the lowest for **1a**•Br^- (−9.6 kcal/mol); the difference between these systems amounts to 27.6 kcal/mol.

In the following, the relative energies are used to visualize the interaction energy maps of the systems **1**•X. Therefore, the energies of the most favorable conformation in the complexes **1**•X are set as 100%. The obtained interaction energy maps of the systems **1**•X are depicted in Figures 3 and S1. A comparison of the maps shows that in the energetically most favored conformations, |α| amounts to 60° and β is

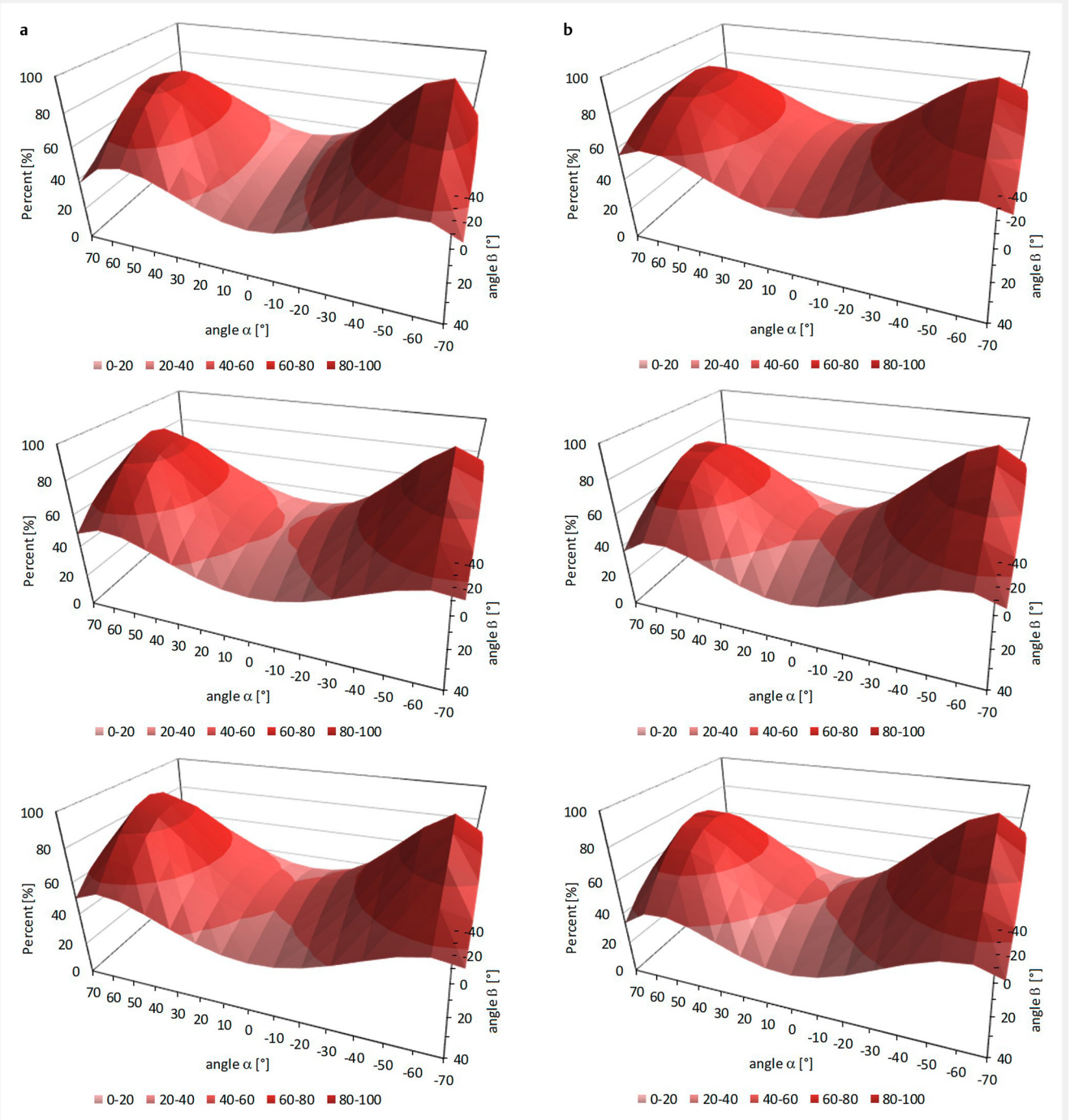

Figure 3 a) Interaction energy maps of the model complexes **1a**•F^- (top), **1a**•Cl^- (center) and **1a**•Br^- (bottom). b) Interaction energy maps of the model complexes **1c**•F^- (top), **1c**•Cl^- (center) and **1c**•Br^- (bottom).

equal to 0°; the anions are therefore found in the plane of the aromatic system and in the imagined extension of the covalent bonds to the chalcogen atom. Interesting is the change of the interaction energy with variation of the angles α and β in dependence of the examined system. For example, the system **1a**•F^- having an angle α of 0° (β is also equal to 0°) exhibits only 32% of the maximum interaction energy (Figure 3a). For **1c**•F^-, on the other hand, it is 50% for this orientation (α = β = 0°; Figure 3b). All systems show a stronger dependence of the energy decrease on the change of α com-

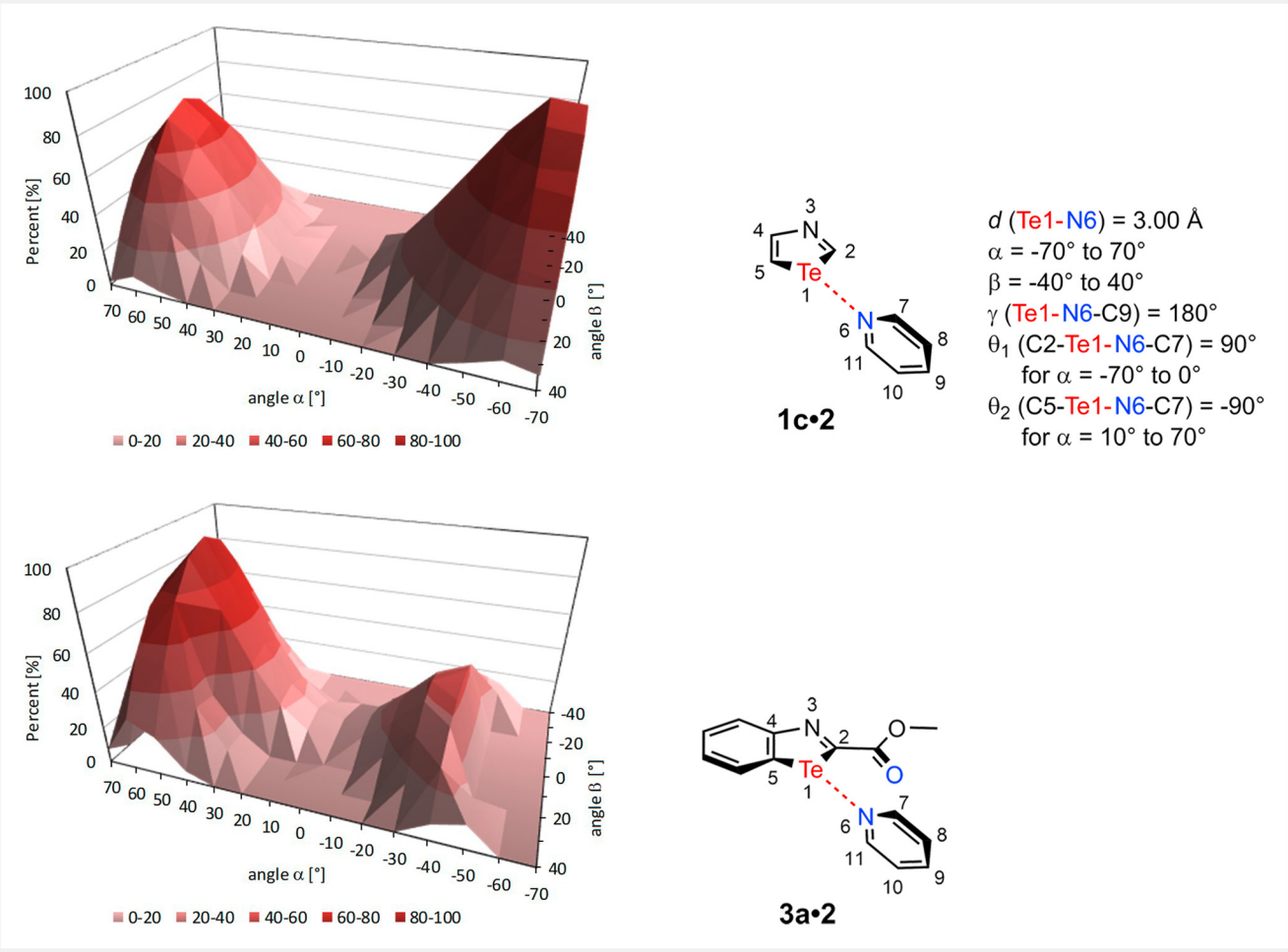

Figure 4 Definitions of the model systems **1c•2** (top) and **3a•2** (bottom) and their interaction energy maps (left).

pared to β. At an angle of α = −60° and β = ±30°, the attractive interaction is still about 70% (in the case of **1c•**F^- even 80%) of the maximum value. Overall, **1c•**F^- shows the smallest changes, i.e. the whole area is very flat, which should in principle allow the interaction of two nucleophilic centers with one σ-hole.

As halides cannot form chelating ligands, we tested if similar interaction energy maps can be found for other nucleophilic centers. Therefore, pyridine was used as a Lewis base because based on this molecule a lot of chelating ligands can be designed. Due to the above-mentioned results, tellurium-containing compounds seemed to be most promising for the intended aim. For this reason, tellurazole **1c** and benzotellurazole **3a** were employed. In the case of the latter, one of the two σ-holes is blocked by the adjacent nucleophilic oxygen, so that the stabilizing interaction of the pyridine should take place only with the other σ-hole. The B2PLYP[45] approximation with additional dispersion correction,[46] which leads for many systems to comparable results with the CCSD(T) method,[7,10,49,50] was applied for model system calculations. Again, the counterpoise method and the basis sets TZVP (for C, H, N, O) and aug-cc-pVTZ-PP (for Te) were employed. The angle γ was fixed to values of 180° to ensure that the lone pair of the nitrogen atom of the pyridine points directly to the tellurium atom (see Figure 4). In addition, the orientation of the two aromatic systems with respect to each other had to be determined; therefore, the angles θ_1 und θ_2 were fixed to values of 90° and −90°, respectively. The thus obtained energies are listed in Tables S10 and S11.

The highest interaction energy amounts to −6.0 kcal/mol for **1c•2** and to −5.7 kcal/mol for **3a•2**. If the interaction energy maps are viewed regarding the relative energies of model systems **1c•2** and **3a•2** (Figure 4), the following can be stated: for both cases, the energy decrease caused by a change of β is not as pronounced as the decrease affected by modification of α. The dependence of the energy on α is strong, so that one finds at an α value of 0° no attractive in-

teraction (in the case of **1c•2**) or only slight (in the case of **3a•2**) attractive interactions. In the case of **3a•2**, the energy at α = 50° and β = ±30° amounts to 52% of the maximum value. This means that a bidentate ligand having two nucleophilic centers arranged in such a way that they can both interact with the σ-hole, where |β| for both is less than 30°, would preferentially form a two-lone-pair/one-σ-hole interaction (2 × > 52%) as compared to a one-lone-pair/one-σ-hole interaction (100%).

We searched the Cambridge Structural Database to check whether a two-lone-pair/one-σ-hole interaction was found for similar systems, but we could not find anything corresponding. However, it becomes evident that the deviations from the ideal geometry are highest for the tellurium-containing compounds, indicating flat interaction energy maps (see Figures S32 and S33).

b) Interactions of Benzochalcogenazoles with N-Containing Chelating Ligands

The above-described promising results of the interaction energy maps prompted us to realize the design of systems, in which a single σ-hole interacts with a chelating ligand that contains two Lewis base centers, by model calculations and lab experiments. For our calculations, the benzotellurazoles **3a** and **4c** were used as chalcogen bond donors (Figure 5). In these compounds, one σ-hole at the chalcogen center is blocked by the adjacent oxygen and accordingly only one is available for the interaction with the chelating ligand. Additionally, **3a** and **4c** offer the advantage that they also represent a chelating ligand with two Lewis base centers. Thus, on the one hand, they can act as chalcogen bond donors, and on the other hand, they are as well chalcogen bond acceptors; this means that a dimerization of **3a** and **4c** can lead to the desired chelate complexes. The monodentate Lewis bases **5, 6** and **7a–d** and the bidentate systems **3a, 4a–d, 8** and **9** were used as chalcogen bond acceptors (Figure 5).

For chalcogen bond calculations, the B3LYP[51–53] method with additional dispersion correction with Becke–Johnson damping[46] (D3BJ) was applied. Again, the counterpoise method and the basis sets TZVP (for C, H, N, O) and aug-cc-pVTZ-PP (for Te) were used. The most important data are summarized in Table 1. Besides the calculations, compounds **3b, 3c** and **4a–c** were synthesized in analogy to already known compounds (Scheme 1). Compounds **3b, 3c** and **4a–c** were crystallized in the presence of different chalcogen bond acceptors. However, only crystals of pure **3b, 3c** and **4a–c** could be isolated. This shows that the dimerization of **3b, 3c** and **4a–c** is energetically highly more favorable than the formation of mixed crystals. The obtained data of the solid-state structures of **3b, 3c** and **4a–c** are given in Table 2.

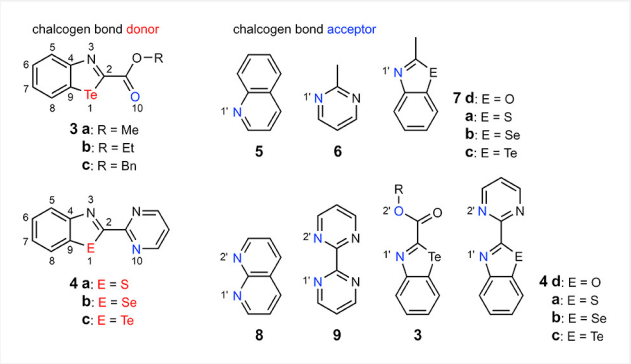

Figure 5 Chalcogen bond donor (left) and acceptor (right) systems used in this study.

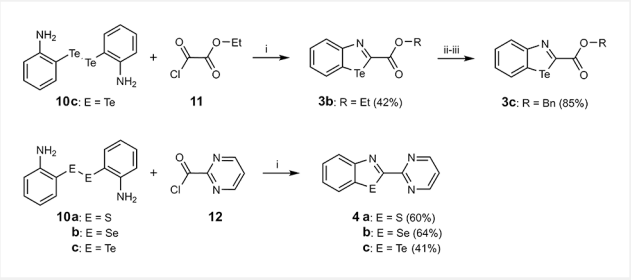

Scheme 1 Synthesis of the model systems **3b, 3c** and **4a–c**. Reaction conditions: i) H_3PO_2, HCl_{conc}, EtOH/THF, Δ; ii) LiOH, H_2O, THF, 10 °C; iii) BnOH, DMAP, DCC, DCM, RT.

First, we consider the calculated complexes of **3a** and **4c** with the monodentate Lewis bases **5, 6** and **7a–d** (Table 1; Figures S2–S7 and S15–S20). These complexes each exhibit only one chalcogen bond. The calculated interaction energies amount to −8 to −9 kcal/mol. The dihedral angles θ_3 and θ_4, which correspond to β in the models **1**•X, **1c•2** and **3a•2**, are normally not significantly differing from 0°. In the case of the acceptor systems **7a–d**, the strength of the chalcogen bond increases with increasing calculated gas-phase basicity of the nitrogen atom in **7** (Tables 1 and S12).

Considering the complexes of **3a** and **4c** with the bidentate Lewis bases **3a, 4a–d, 8** and **9** (Table 1; Figures S8–S14 and S21–S27), it turns out that the complexes of naphthyridine (**8**) exhibit the lowest binding energies. These energies are similarly high to those of the complexes with monodentate ligands. This is in accordance with the fact that only one nitrogen atom forms a chalcogen bond with the tellurium atom. The distance of the second nitrogen atom to tellurium is significantly higher (3.9 Å and 4.5 Å, respectively) than the sum of the van der Waals radii of the two atoms (3.61 Å). This arrangement can presumably be ascribed to the fact that the bite angle in naphthyridines is not suitable for the formation of two equivalent chalcogen bonds.

Table 1 Calculated dihedral angles θ_3(C8–C9-E1-N1′) and θ_4(C8–C9-E1-N2′/O2′) [°], chalcogen bond distances d_1(E1-N10/O10), d_2(E1-N1′) and d_3(E1-N2′/O2′) [Å] as well as binding energies ΔE [kcal/mol] of the investigated complexes by means of B3LYP-D3BJ/TZVP,aug-cc-pVTZ-PP. For numbering, see Figure 5

Complex	Type	d_1 [Å]	d_2 [Å]	d_3 [Å]	θ_3 [°]	θ_4 [°]	ΔE [kcal/mol]
3a•5		3.242	3.061		−2		−8.8
3a•6		3.236	3.096		−4		−7.8
3a•7d		3.236	3.121		−10		−8.0
3a•7a		3.237	3.105		−5		−8.5
3a•7b		3.236	3.114		3		−8.6
3a•7c		3.236	3.134		2		−8.8
3a•8		3.247	3.118	3.895	11	−25	−8.7
3a•9	C	3.243	3.216	3.412	23	−26	−10.7
3a•3a	C	3.234	3.231	3.489	9	−39	−10.0
3a•4d		3.243	3.187	3.589	7	−41	−10.0
3a•4a	C	3.243	3.209	3.494	15	−34	−10.8
3a•4b	C	3.242	3.234	3.461	20	−30	−11.0
3a•4c	C	3.241	3.277	3.397	24	−26	−11.3
4c•5		3.131	3.106		−3		−7.9
4c•6		3.127	3.141		−5		−7.1
4c•7d		3.122	3.192		−12		−7.3
4c•7a		3.126	3.142		5		−7.9
4c•7b		3.124	3.156		−6		−8.0
4c•7c		3.124	3.169		2		−8.1
4c•8		3.134	3.242	4.520	19	−6	−7.6
4c•9		3.123	3.303	3.761	3	47	−9.8
4c•3a	C	3.122	3.259	3.528	8	−39	−9.4
4c•4d		3.131	3.230	3.616	6	−42	−9.0
4c•4a	C	3.131	3.235	3.541	15	−34	−9.9
4c•4b	C	3.130	3.257	3.517	20	−29	−10.1
4c•4c	C	3.129	3.298	3.451	25	−25	−10.4
4a•4a		2.932	4.999	3.560	1	−22	−7.1
4b•4b		3.003	3.245	3.590	25	−24	−8.5

In systems with more favorable bite angles (**3a, 4a–d** and **9**), the distances of the nucleophilic centers to the tellurium atom are smaller and, in many cases, even smaller than the sum of the van der Waals radii of the two atoms so that in the latter case it can be spoken of two chalcogen bonds to one single σ-hole. Here, the comparison of the systems **3a•4a–d** and **4c•4a–d** considering the calculated gas-phase basicity of the nitrogen atoms in **4** (Table S12) is interesting.

The following tendency can be observed: the higher the calculated gas-phase basicity of the nitrogen atoms in **4**, the more stable is the complex and the smaller is the difference of the distances between the tellurium atom (Te1) and the nucleophilic centers (N1′ and N2′). For example, in complex **4c•4 d**, which contains benzotellurazole (**4c**) as the donor and benzoxazole (**4 d**) as the acceptor, the distance d_2(E1-N1′) amounts to 3.23 Å and is significantly smaller than d_3 (E1-N2′) with 3.62 Å (Figure 6a). Whereas N1′ with $\theta_3 = 6°$ is almost located in the aromatic plane, N2′ with $\theta_4 = -42°$ lies significantly above the plane. Considering that the dihedral angles θ_3 and θ_4 correspond to β in model **3a•2** (Figure 4), the interaction energy between the Te1 and N2′ center ($\theta_4 = -42°$) can be estimated to ca. 20% of the maximum chalcogen bond energy. However, the chalcogen bond between the centers Te1 and N1′ ($\theta_3 = 0°$) almost represents an ideal chalcogen bond. This means, in **3a•2** the second Lewis center (N2′) leads to an additional stabilization of about 20% of the maximum chalcogen bond energy.

A contrary picture can be found for complex **4c•4c** consisting of two identical benzotellurazole units (Figure 6b): the calculated distances d_2(E1-N1′) and d_3(E1-N2′) differ only slightly (3.30 Å and 3.45 Å); one nitrogen atom lies below the plane ($\theta_3 = 25°$), whereas the other is located above the

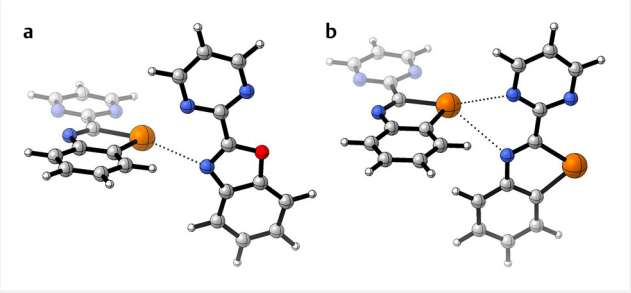

Figure 6 Ball and stick representations (CYLview20[54]) of the molecular structures of the complexes **4c•4d** (a) and **4c•4c** (b; type C) calculated by means of B3LYP-D3BJ/TZVP,aug-cc-pVTZ-PP. Color codes: grey, carbon; white, hydrogen; brown, tellurium; blue, nitrogen; red, oxygen (dashed black lines denote chalcogen bonds at the examined center).

plane ($\theta_4 = -25°$) (Figure 6b). This means both nitrogen atoms form chalcogen bonds to the same σ-hole. These bonds are energetically equivalent, which corresponds to the description of type C. If model **3a•2** (Figure 4) is again considered for comparison, it can be recognized that for $\beta = 25°$ (or $-25°$) the energy value found amounts to 60–70% of an ideal chalcogen bond.

To evaluate whether the three-center interaction in **4c•4c** is substantially different from two-center chalcogen bonding, energy decomposition analyses[55] (B3LYP-D3BJ/QZ4P) were performed for **4c•4c** and **4c•7c**. Comparison shows that both are very similar. In **4c•7c**, the term of electrostatic interaction to the total attractive interaction is slightly higher (**4c•4c:** 41%, **4c•7c:** 45%), while the fraction of dispersion energy is lower (**4c•4c:** 38%, **4c•7c:** 35%). The term of total orbital interactions is the same in both cases (21%).

The experimental confirmation for type C can be found in the solid-state structures of **3b•3b, 3c•3c** and **4c•4c** (Table 2, and Figures 7, S30 and S31). The distances between the nucleophilic centers and the tellurium atom (d_2(E1-N1′) and d_3(E1-N2′/O2′)) differ only slightly. Moreover, one center is located significantly above and one significantly below the aromatic plane (Figure 7c). Thus, both nucleophilic centers form almost equivalent chalcogen bonds to one single σ-hole. For the selenium-containing dimer **4b•4b**, a similar conformation to that of complex **4c•4 d** is found: one nitrogen atom forms an almost ideal chalcogen bond while the second one only causes an additional stabilization (Figure 7b). The Se1–N2′ distance (3.48 Å) is therefore larger than the sum of the van der Waals radii of the two atoms (3.45 Å). In the sulfur-containing dimer **4a•4a**, only one N atom of the acceptor forms a chalcogen bond (Figure 7a).

Table 2 Measured dihedral angles θ_3(C8–C9-E1-N1′) and θ_4(C8–C9-E1-N2′/O2′) [°], and chalcogen bond distances d_1(E1-N10/O10), d_2(E1-N1′) and d_3(E1-N2′/O2′) [Å] of the dimeric complexes **3b•3b, 3c•3c, 4a•4a, 4b•4b** and **4c•4c**. For numbering, see Figure 5.

Complex	Type	d_1 [Å]	d_2 [Å]	d_3 [Å]	θ_3 [°]	θ_4 [°]
3b•3b	C	3.235	3.158	3.374	14	−36
	C	3.225	3.301	3.538	−16	31
3c•3c	C	3.243	3.416	3.406	30	−16
4a•4a		2.853	4.531	3.184	13	18
4b•4b		2.978	3.480	3.425	29	−16
4c•4c	C	3.154	3.344	3.288	20	−24

Conclusions

In this work interaction energy maps for chalcogen bonds between chalcogenazoles and Lewis bases were calculated by quantum chemical methods. It becomes evident that two-lone-pair/one-σ-hole interactions should in principle be possible for tellurium-containing compounds, since a change in the attractive interaction is not very pronounced when deviating from planarity. These assumptions were proven by quantum chemical calculations and X-ray studies.

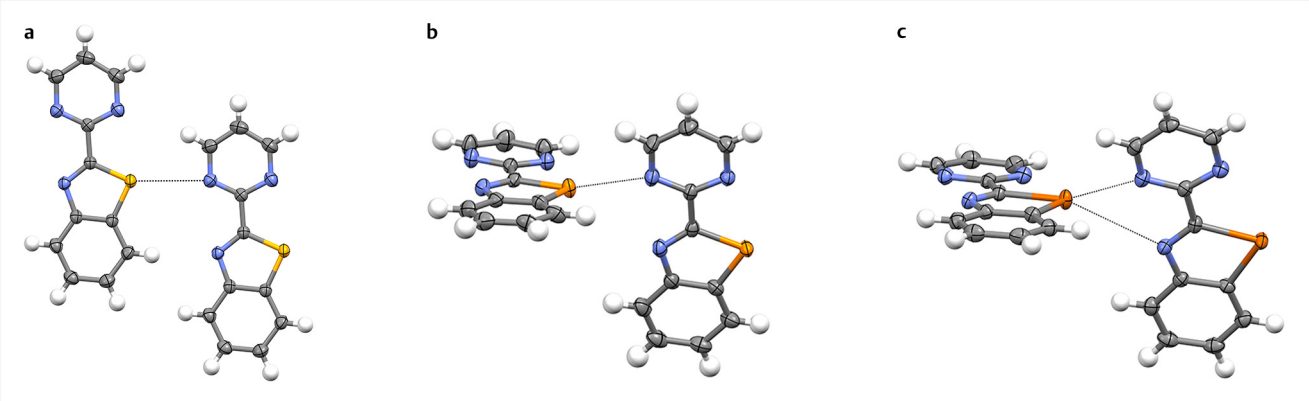

Figure 7 Molecular structures of the dimeric complexes **4a•4a** (a), **4b•4b** (b) and **4c•4c** (c, type C) in the solid state. Ellipsoids are set at 75% probability (dashed black lines denote chalcogen bonds at the examined center).

The higher the calculated gas-phase basicity of the nucleophilic center, the more likely is the formation of bifurcated chalcogen bonds. The studied two-lone-pair/one-σ-hole interaction fixes the relative orientation of the molecules in the complex. Thus, these bond types are promising with respect to the formation of more complex and more rigid structures based on chalcogen interactions.

Experimental Section

General remarks. All chemicals were of reagent grade and used without further purification. Reactions were monitored by TLC analysis with silica gel 60 F254 thin-layer plates. Flash chromatography was carried out on silica 60 (40–63 µm, 230–400 mesh). ^{1}H, ^{13}C and ^{125}Te NMR spectra were measured with Bruker Avance DRX 400, 500 and Avance HD 600 spectrometers. All chemical shifts (δ) are given in ppm. The spectra were referenced to the peak for the protium impurity in the deuterated solvents indicated in brackets in the analytical data. Signal multiplicity for ^{1}H NMR was determined as s (singlet), d (doublet), t (triplet), sext (sextet), sept (septet), m (multiplet), dd (doublet of doublets) and td (triplet of doublets). ^{13}C NMR spectra were measured with ^{1}H decoupling and the ^{13}C assignment was achieved via DEPT 135, HSQC, HMBC, and COSY spectra. ^{13}C signal multiplicity was determined as p (primary), s (secondary), t (tertiary), q (quaternary). HR-MS spectra were recorded with a Bruker BioTOF III Instrument with ESI as ionization source. UV/Vis absorption spectra were obtained with a Jasco V-550 spectrophotometer. Ditelluride **10c**[56] and diselenide **10b**[57] were synthesized according to known procedures. Disulfide **10a** was purchased from Alfa Aesar.

Procedures

General procedure for the synthesis of the benzoazoles 3b (R = Et) and 4a–c. To a solution of disulfide (**10a**), diselenide (**10b**), or ditelluride (**10c**) in THF (8 mL/mmol starting material), acid chloride (**11** or **12**) (2.1 equiv) was added and the mixture was stirred for 5 min. Afterwards, 50% aq. hypophosphorous acid (0.2 mL/mmol starting material) was added and the solution was stirred for 5 min at room temperature. This step was followed by an addition of 95% ethanol (3.2 mL/mmol starting material) and 36% hydrochloric acid (2 mL/mmol starting material). The resulting mixture was heated to reflux for 1–2 hours. After cooling to room temperature, the mixture was chilled in an ice bath for 30 min. Ammonia solution (5% aq.) was added to the cooled mixture to basify to pH = 8 and the solution was repeatedly extracted with DCM. The organic layers were combined, dried over $MgSO_4$, and concentrated in vacuo. The residue was purified by chromatography on silica gel to provide the desired product.

Synthesis of benzotellurazole 3b (R = Et). This compound was synthesized according to the mentioned applied procedure from ditelluride **10c** (1.46 g, 3.32 mmol) and acid chloride **11** (956 mg, 7 mmol). After flash column chromatography with silica gel (*n*-pentane/EtOAc 6:1), benzotellurazole **3b** was obtained as a yellow solid (900 mg, 2.97 mmol, 42%). M. p. 77–79 °C.

IR (ATR): 2976, 1692, 1493, 1279, 1256, 1053, 766 cm^{-1}.

^{1}H NMR (400 MHz, $CDCl_3$): δ = 8.43–8.41 (m, 1 H; $C_{ar}H$), 7.97–7.95 (m, 1 H; $C_{ar}H$), 7.53–7.49 (m, 1 H; $C_{ar}H$), 7.28–7.24 (m, 1 H; $C_{ar}H$), 4.48 (q, 2 H; CO_2CH_2), 1.44 ppm (t, 3 H; CH_2CH_3).

^{13}C NMR (101 MHz, $CDCl_3$): δ = 165.8 (q; C_{ar}), 165.7 (q; CO), 161.5 (q; C_{ar}), 137.7 (t; C_{ar}), 132.0 (q; C_{ar}), 129.5 (t; C_{ar}), 127.5 (t; C_{ar}), 126.8 (t; C_{ar}), 63.4 (s; CH_2CH_3), 14.4 ppm (p; CH_2CH_3).

^{125}Te NMR (126 MHz, $CDCl_3$): δ = 976.5 ppm.

HRMS (ESI-TOF): *m*/*z* [M + H]$^+$ calcd for $C_{10}H_{10}NO_2{}^{130}Te^+$: 305.9768; found: 305.9777.

UV/Vis (CH_3CN): λ_{max} (log ε) = 247 (4.14), 296 nm (3.93).

Synthesis of benzotellurazole 3 d (R = H). Benzotellurazole **3b** (605 mg, 2 mmol) was dissolved in THF (2 mL) and the solution was cooled to 10 °C. LiOH•H_2O (84 mg, 2 mmol) in water (4 mL) was added at this temperature and the mixture was stirred for 1 h. Afterwards, dilute hydrochloric acid (1 N) was added dropwise until precipitation appeared. The solid was filtered and dried under vacuum to afford the desired benzotellurazole **3 d** as a yellow powder (500 mg, 1.82 mmol, 91%). M. p. 134–136 °C.

IR (ATR): 2959, 2849, 1694, 1506, 1250, 1049, 760 cm^{-1}.

^{1}H NMR (400 MHz, d_6-DMSO): δ = 13.94 (brs, 1 H, CO_2H), 8.28 (dd, $^{3}J_{H,H}$ = 8.4 Hz, $^{4}J_{H,H}$ = 0.8 Hz, 1 H; $C_{ar}H$), 8.24 (dd, $^{3}J_{H,H}$ = 8.4 Hz, $^{4}J_{H,H}$ = 0.8 Hz, 1 H; $C_{ar}H$), 7.59–7.55 (m, 1 H; $C_{ar}H$), 7.36–7.31 ppm (m, 1 H; $C_{ar}H$).

^{13}C NMR (101 MHz, d_6-DMSO): δ = 170.1 (q; C_{ar}), 167.3 (q; CO), 161.3 (q; C_{ar}), 136.9 (t; C_{ar}), 133.1 (q; C_{ar}), 128.3 (t; C_{ar}), 127.2 (t; C_{ar}), 126.1 ppm (t; C_{ar}).

^{125}Te NMR (126 MHz, d_6-DMSO): δ = 968.6 ppm.

HRMS (ESI-TOF): *m*/*z* [M + H]$^+$ calcd for $C_8H_6NO_2{}^{130}Te^+$: 277.9455; found: 277.9464.

UV/Vis (THF): λ_{max} (log ε) = 369 nm (3.25).

Synthesis of benzotellurazole 3c (R = Bn). To a solution of benzotellurazole **3 d** (274 mg, 1 mmol), benzyl alcohol (135 mg, 1.25 mmol), and 4-dimethylaminopyridine (DMAP; 24.40 mg, 0.2 mmol) in dichloromethane (7 mL), *N*, *N*′-dicyclohexylcarbodiimide (DCC; 1 mmol, 206 mg) was added and the solution was stirred at room temperature until TLC showed consumption of starting material (1 h). Then, the solution was concentrated in vacuo and the residue was repeatedly extracted with ethyl acetate, HCl (1 N) and water. The combined organic phases were washed with saturated $NaHCO_3$ and brine, dried over $MgSO_4$ and concentrated in

vacuo. The residue was purified by flash column chromatography with silica gel (*n*-pentane/EtOAc 5 : 1), and benzotellurazole **3c** was obtained as a yellow solid (310 mg, 0.85 mmol, 85%). M. p. 114–116 °C.

IR (ATR): 3069, 2961, 1701, 1489, 1248, 1043, 766 cm^{-1}.

^1H NMR (400 MHz, $CDCl_3$): δ = 8.45 (dd, $^3J_{H,H}$ = 8.4 Hz, $^4J_{H,H}$ = 0.8 Hz, 1 H; $C_{ar}H$), 7.99 (d, $^3J_{H,H}$ = 8.0 Hz, 1 H; $C_{ar}H$), 7.57–7.53 (m, 1 H; $C_{ar}H$), 7.51–7.48 (m, 2 H; $C_{ar}H$, $C_{ar}H$), 7.42–7.36 (m, 3 H; $C_{ar}H$, $C_{ar}H$, $C_{ar}H$), 7.32–7.28 (m, 1 H; $C_{ar}H$), 5.48 ppm (s, 2 H; OCH_2).

^{13}C NMR (101 MHz, $CDCl_3$): δ = 165.6 (q; C_{ar}), 165.5 (q; CO), 161.5 (q; C_{ar}), 137.9 (t; C_{ar}), 135.1 (q; C_{ar}), 132.0 (q; C_{ar}), 129.6 (t; C_{ar}), 128.8 (t; C_{ar}), 127.6 (t; C_{ar}), 127.0 (t; C_{ar}), 68.8 ppm (s; OCH_2Ph).

^{125}Te NMR (126 MHz, $CDCl_3$): δ = 980.9 ppm.

HRMS (ESI-TOF): *m*/*z* $[M + H]^+$ calcd for $C_{15}H_{12}NO_2{}^{130}Te^+$: 367.9925; found: 367.9885.

UV/Vis (CH_3CN): λ_{max} (log ε) = 247 (4.17), 297 nm (3.96).

Synthesis of benzothiazole 4a. This compound was synthesized according to the general procedure from disulfide **10a** (174 mg, 0.7 mmol) and acid chloride **12** (210 mg, 1.47 mmol). After flash column chromatography with silica gel (*n*-pentane/EtOAc 1 : 2), benzothiazole **4a** was obtained as a white solid (190 mg, 0.89 mmol, 60%). M. p. 128–130 °C.

IR (ATR): 3046, 1557, 1504, 1406, 1317, 1015, 762 cm^{-1}.

^1H NMR (400 MHz, $CDCl_3$): δ = 8.93–8.90 (m, 2 H; $C_{pyrimidine}H$, $C_{pyrimidine}H$), 8.25 (dd, $^3J_{H,H}$ = 8.0 Hz, $^4J_{H,H}$ = 1.6 Hz, 1 H; $C_{ar}H$), 7.99–7.95 (m, 1 H; $C_{ar}H$), 7.55–7.51 (m, 1 H; $C_{ar}H$), 7.49–7.44 (m, 1 H; $C_{ar}H$), 7.38–7.34 ppm (m, 1 H; $C_{pyrimidine}H$).

^{13}C NMR (101 MHz, $CDCl_3$): δ = 166.6 (q; C_{ar}), 160.0 (q; $C_{pyrimidine}$), 158.0 (t; $C_{pyrimidine}$), 154.4 (q; C_{ar}), 136.6 (q; C_{ar}), 126.8 (t; C_{ar}), 126.7 (t; C_{ar}), 125.0 (t; C_{ar}), 122.1 (t; C_{ar}), 121.5 ppm (t; $C_{pyrimidine}$).

HRMS (ESI-TOF): *m*/*z* $[M + H]^+$ calcd for $C_{11}H_8N_3S^+$: 214.0433; found: 214.0419.

UV/Vis (CH_3CN): λ_{max} (log ε) = 224 (4.28), 299 nm (4.21).

Synthesis of benzoselenazole 4b. This compound was synthesized according to the general procedure from diselenide **10b** (225 mg, 0.66 mmol) and acid chloride **12** (200 mg, 1.40 mmol). After flash column chromatography with silica gel (*n*-pentane/EtOAc 1 : 2), benzoselenazole **4b** was obtained as a white solid (232 mg, 0.89 mmol, 64%). M. p. 163–165 °C.

IR (ATR): 3055, 1557, 1512, 1406, 1078, 974, 758 cm^{-1}.

^1H NMR (600 MHz, $CDCl_3$): δ = 8.90 (d, $^3J_{H,H}$ = 4.8 Hz, 2 H; $C_{pyrimidine}H$, $C_{pyrimidine}H$), 8.32 (d, $^3J_{H,H}$ = 8.4 Hz, 1 H; $C_{ar}H$), 8.00 (d, $^3J_{H,H}$ = 7.8 Hz, 1 H; $C_{ar}H$), 7.53–7.50 (m, 1 H; $C_{ar}H$), 7.36 ppm (t, $^3J_{H,H}$ = 4.8 Hz, 1 H; $C_{pyrimidine}H$).

^{13}C NMR (151 MHz, $CDCl_3$): δ = 172.1 (q; C_{ar}), 161.7 (q; $C_{pyrimidine}$), 158.0 (t; $C_{pyrimidine}$), 156.3 (q; C_{ar}), 140.0 (q; C_{ar}), 126.8 (t; C_{ar}), 126.7 (t; C_{ar}), 126.6 (t; C_{ar}), 125.2 (t; C_{ar}), 121.4 ppm (t; $C_{pyrimidine}$).

^{77}Se NMR (114 MHz, $CDCl_3$): δ = 658.2 ppm.

HRMS (ESI-TOF): *m*/*z* $[M + H]^+$ calcd for $C_{11}H_8N_3{}^{80}Se^+$: 261.9878; found: 261.9871.

UV/Vis (CH_3CN): λ_{max} (log ε) = 231 (4.24), 301 nm (4.14).

Synthesis of benzotellurazole 4c. This compound was synthesized according to the general procedure from ditelluride **10c** (351 mg, 0.80 mmol) and acid chloride **12** (241 mg, 1.70 mmol). After flash column chromatography with silica gel (*n*-pentane/EtOAc 1 : 2), benzotellurazole **4c** was obtained as a yellow solid (215 mg, 0.70 mmol, 41%). M. p. 216–218 °C.

IR (ATR): 2918, 1557, 1555, 1501, 1408, 1310. 961, 764 cm^{-1}.

^1H NMR (400 MHz, $CDCl_3$): δ = 8.87 (d, $^3J_{H,H}$ = 4.8 Hz, 2 H; $C_{pyrimidine}H$, $C_{pyrimidine}H$), 8.44 (dd, $^3J_{H,H}$ = 8.0 Hz, $^3J_{H,H}$ = 1.2 Hz, 1 H; $C_{ar}H$), 7.99 (dd, $^3J_{H,H}$ = 8.0 Hz, $^3J_{H,H}$ = 1.2 Hz, 1 H; $C_{ar}H$), 7.54–7.50 (m, 1 H; $C_{ar}H$), 7.35 (t, $^3J_{H,H}$ = 4.8 Hz, 1 H; $C_{pyrimidine}H$), 7.27–7.22 ppm (m, 1 H; $C_{ar}H$).

^{13}C NMR (101 MHz, $CDCl_3$): δ = 175.3 (q; C_{ar}), 165.6 (q; $C_{pyrimidine}$), 163.1 (q; C_{ar}), 158.2 (t; $C_{pyrimidine}$), 136.3 (t; C_{ar}), 131.9 (q; C_{ar}), 128.8 (t; C_{ar}), 127.2 (t; C_{ar}), 126.1 (t; C_{ar}), 121.1 ppm (t; $C_{pyrimidine}$).

^{125}Te NMR (126 MHz, $CDCl_3$): δ = 918.4 ppm.

HRMS (ESI-TOF): *m*/*z* $[M + H]^+$ calcd for $C_{11}H_8N_3{}^{130}Te^+$: 311.9775; found: 311.9776.

UV/Vis (CH_3CN): λ_{max} (log ε) = 251 (4.17), 310 nm (4.05).

Funding Information

This work was supported by the Deutsche Forschungsgemeinschaft (DFG; HA 2973/15–1).

Supporting Information

Figures and tables, Cambridge Structural Database (CSD) search, computational details, Cartesian coordinates and absolute energies for all calculated compounds, crystal structure data (CCDC numbers: 2062726–2062730) and NMR spectra of the new compounds are included in the Supporting Information for this article, available online at https://doi.org/10.1055/a-1883-6076.

Conflict of Interest

The authors declare no conflict of interest.

References

(1) Kolb, S.; Oliver, G. A.; Werz, D. B. *Angew. Chem. Int. Ed.* **2020**, *59*, 22306.

(2) Aakeroy, C. B.; Bryce, D. L.; Desiraju, G. R.; Frontera, A.; Legon, A. C.; Nicotra, F.; Rissanen, K.; Scheiner, S.; Terraneo, G.; Metrangolo, P.; Resnati, G. *Pure Appl. Chem*. **2019**, *91*, 1889.
(3) Biot, N.; Bonifazi, D. *Chem. Eur. J*. **2020**, *26*, 2904.
(4) Kumar, V.; Xu, Y.; Bryce, D. L. *Chem. Eur. J*. **2020**, *26*, 3275.
(5) Ho, P. C.; Wang, J. Z.; Meloni, F.; Vargas-Baca, I. *Coord. Chem. Rev*. **2020**, *422*, 213464.
(6) Scilabra, P.; Terraneo, G.; Resnati, G. *Acc. Chem. Res*. **2019**, *52*, 1313.
(7) Gleiter, R.; Haberhauer, G.; Werz, D. B.; Rominger, F.; Bleiholder, C. *Chem. Rev*. **2018**, *118*, 2010.
(8) Cozzolino, A. F.; Elder, P. J. W.; Vargas-Baca, I. *Coord. Chem. Rev*. **2011**, *255*, 1426.
(9) Werz, D. B.; Gleiter, R.; Rominger, F. *Organometallics* **2003**, *22*, 843.
(10) Mehrparvar, S.; Wölper, C.; Gleiter, R.; Haberhauer, G. *Angew. Chem. Int. Ed*. **2020**, *59*, 17154.
(11) Eckstein, B. J.; Brown, L. C.; Noll, B. C.; Moghadasnia, M. P.; Balaich, G. J.; McGuirk, C. M. *J. Am. Chem. Soc*. **2021**, *143*, 20207.
(12) Navarro-García, E.; Galmés, B.; Velasco, M. D.; Frontera, A.; Caballero, A. *Chem. Eur. J*. **2020**, *26*, 4706.
(13) Borissov, A.; Marques, I.; Lim, J. Y. C.; Félix, V.; Smith, M. D.; Beer, P. D. *J. Am. Chem. Soc*. **2019**, *141*, 4119.
(14) Riwar, L.-J.; Trapp, N.; Root, K.; Zenobi, R.; Diederich, F. *Angew. Chem. Int. Ed*. **2018**, *57*, 17259.
(15) Chen, L.; Xiang, J.; Zhao, Y.; Yan, Q. *J. Am. Chem. Soc*. **2018**, *140*, 7079.
(16) Lim, J. Y. C.; Marques, I.; Thompson, A. L.; Christensen, K. E.; Félix, V.; Beer, P. D. *J. Am. Chem. Soc*. **2017**, *139*, 3122.
(17) Ho, P. C.; Szydlowski, P.; Sinclair, J.; Elder, P. J. W.; Kübel, J.; Gendy, C.; Lee, L. M.; Jenkins, H.; Britten, J. F.; Morim, D. R.; Vargas-Baca, I. *Nat. Commun*. **2016**, *7*, 11299.
(18) Benz, S.; Macchione, M.; Verolet, Q.; Mareda, J.; Sakai, N.; Matile, S. *J. Am. Chem. Soc*. **2016**, *138*, 9093.
(19) Macchione, M.; Goujon, A.; Strakova, K.; Humeniuk, H. V.; Licari, G.; Tajkhorshid, E.; Sakai, N.; Matile, S. *Angew. Chem. Int. Ed*. **2019**, *58*, 15752.
(20) Mehrparvar, S.; Scheller, Z. N.; Wölper, C.; Haberhauer, G. *J. Am. Chem. Soc*. **2021**, *143*, 19856.
(21) Young, C. M.; Elmi, A.; Pascoe, D. J.; Morris, R. K.; McLaughlin, C.; Woods, A. M.; Frost, A. B.; de la Houpliere, A.; Ling, K. B.; Smith, T. K.; Slawin, A. M. Z.; Willoughby, P. H.; Cockroft, S. L.; Smith, A. D. *Angew. Chem. Int. Ed*. **2020**, *59*, 3705.
(22) Wang, W.; Zhu, H.; Feng, L.; Yu, Q.; Hao, J.; Zhu, R.; Wang, Y. *J. Am. Chem. Soc*. **2020**, *142*, 3117.
(23) Wonner, P.; Steinke, T.; Vogel, L.; Huber, S. M. *Chem. Eur. J*. **2020**, *26*, 1258.
(24) Strakova, K.; Assies, L.; Goujon, A.; Piazzolla, F.; Humeniuk, H. V.; Matile, S. *Chem. Rev*. **2019**, *119*, 10977.
(25) Wang, W.; Zhu, H.; Liu, S.; Zhao, Z.; Zhang, L.; Hao, J.; Wang, Y. *J. Am. Chem. Soc*. **2019**, *141*, 9175.
(26) Wonner, P.; Dreger, A.; Vogel, L.; Engelage, E.; Huber, S. M. *Angew. Chem. Int. Ed*. **2019**, *58*, 16923.
(27) Benz, S.; Poblador-Bahamonde, A. I.; Low-Ders, N.; Matile, S. *Angew. Chem. Int. Ed*. **2018**, *57*, 5408.
(28) Mahmudov, K. T.; Kopylovich, M. N.; Guedes da Silva, M. F. C.; Pombeiro, A. J. L. *Dalton Trans*. **2017**, *46*, 10121.
(29) Politzer, P.; Murray, J. S.; Clark, T.; Resnati, G. *Phys. Chem. Chem. Phys*. **2017**, *19*, 32166.
(30) Clark, T. *WIREs Comput. Mol. Sci*. **2013**, *3*, 13.
(31) Haberhauer, G.; Gleiter, R. *Angew. Chem. Int. Ed*. **2020**, *59*, 21236.
(32) Bleiholder, C.; Gleiter, R.; Werz, D. B.; Köppel, H. *Inorg. Chem*. **2007**, *46*, 2249.
(33) Bleiholder, C.; Werz, D. B.; Köppel, H.; Gleiter, R. *J. Am. Chem. Soc*. **2006**, *128*, 2666.
(34) Ho, P. C.; Rafique, J.; Lee, J.; Lee, L. M.; Jenkins, H. A.; Britten, J. F.; Braga, A. L.; Vargas-Baca, I. *Dalton Trans*. **2017**, *46*, 6570.
(35) Garrett, G. E.; Gibson, G. L.; Straus, R. N.; Seferos, D. S.; Taylor, M. S. *J. Am. Chem. Soc*. **2015**, *137*, 4126.
(36) Cozzolino, A. F.; Vargas-Baca, I.; Mansour, S.; Mahmoudkhani, A. H. *J. Am. Chem. Soc*. **2005**, *127*, 3184.
(37) Smith, W. E.; Franklin, D. V.; Goutierrez, K. L.; Fronczek, F. R.; Mautner, F. A.; Junk, T. *Am. J. Heterocycl. Chem*. **2019**, *5*, 49.
(38) Kremer, A.; Fermi, A.; Biot, N.; Wouters, J.; Bonifazi, D. *Chem. Eur. J*. **2016**, *22*, 5665.
(39) Biot, N.; Bonifazi, D. Coord. *Chem. Rev*. **2020**, *413*, 213243.
(40) Pascoe, D. J.; Ling, K. B.; Cockroft, S. L. *J. Am. Chem. Soc*. **2017**, 139, 15160.
(41) Mahmudov, K. T.; Aliyeva, V. A.; Guedes da Silva, M. F. C.; Pombeiro, A. J. L. In *Halogen Bonding in Solution*; Huber, S.; Wiley-VCH: Weinheim, **2021**.
(42) Rozas, I.; Alkorta, I.; Elguero, J. *J. Phys. Chem. A* **1998**, *102*, 9925.
(43) Ji, B.; Wang, W.; Deng, D.; Zhang, Y. *Cryst. Growth Des*. **2011**, *11*, 3622.
(44) Scheiner, S. *Molecules* **2021**, *26*, 350.
(45) Grimme, S. *J. Chem. Phys*. **2006**, *124*, 034108.
(46) Grimme, S.; Ehrlich, S.; Goerigk, L. *J. Comput. Chem*. **2011**, *32*, 1456.
(47) Purvis III, G. D.; Bartlett, R. J. *J. Chem. Phys*. **1982**, *76*, 1910.
(48) Boys, S. F.; Bernardi, F. *Mol. Phys*. **1970**, *19*, 553.
(49) Fabig, S.; Haberhauer, G.; Gleiter, R. *J. Am. Chem. Soc*. **2015**, *137*, 1833.
(50) Haberhauer, G.; Gleiter, R. *J. Am. Chem. Soc*. **2013**, *135*, 8022.
(51) Miehlich, B.; Savin, A.; Stoll, H.; Preuss, H. *Chem. Phys. Lett*. **1989**, *157*, 200.
(52) Becke, A. D. *Phys. Rev. A* **1988**, *38*, 3098.
(53) Lee, C.; Yang, W.; Parr, R. G. *Phys. Rev. B: Condens. Matter* **1988**, *37*, 785.
(54) Legault, C. Y. CYLview20, Université de Sherbrooke, **2020**.
(55) Bickelhaupt, F. M.; Baerends, E. J. *Rev. Comput. Chem*. **2000**, *15*, 1.
(56) McMullen, N. C.; Fronczek, F. R.; Junk, T. *J. Heterocycl. Chem*. **2013**, *50*, 120.
(57) Kremer, A.; Aurisicchio, C.; De Leo, F.; Ventura, B.; Wouters, J.; Armaroli, N.; Barbieri, A.; Bonifazi, D. *Chem. Eur. J*. **2015**, *21*, 15377.